Modern Physics Letters B 2050398 (14 pages) © World Scientific Publishing Company DOI: 10.1142/S0217984920503984



The analysis of electron scattering among multiplying layer in EBAPS using optimized Monte Carlo method

Jinzhou Bai*,^{†,¶}, Yonglin Bai*,[∥], Xun Hou*, Weiwei Cao*,^{†,§}, Yang Yang*, Bo Wang*, Xiaohong Bai* and Siqi Li^{†,‡}

*Key Laboratory of Ultrafast Photoelectric Diagnostic Technology,
Xi'an Institute of Optics and Precision Mechanics,
Chinese Academy of Sciences (CAS), Xi'an 710119, P. R. China

† University of Chinese Academy of Sciences (UCAS),
Beijing 100049, P. R. China

‡ State Key Laboratory of Transient Optics and Photonics,
Xi'an Institute of Optics and Precision Mechanics,
Chinese Academy of Sciences (CAS), Xi'an 710119, P. R. China

§ Key Laboratory for Physical Electronics and Devices of the Ministry
of Education and Shaanxi Key Laboratory of Information Photonic Technique,
Xi'an Jiaotong University, Xi'an 710049, P. R. China

¶ Collaborative Innovation Center of Extreme Optics,
Shanxi University, Taiyuan 030006, Shanxi, P. R. China

µ baiyonglin@opt.ac.cn

Received 11 April 2020 Revised 2 June 2020 Accepted 2 June 2020 Published 25 September 2020

Electron bombarded Active Pixel Sensor (EBAPS) is well known for its low noise in low-light level imaging, high mechanical integration, and a relatively low cost. It plays an important role in areas of the industrial process as well as the fundamental scientific research. However, the performance of EBAPS is intensively influenced by the structural parameters (i.e. the acceleration voltage between cathode and anode, thickness of the passivation layer, etc.). Due to the influence of these factors mentioned above, the performance of EBAPS is restricted to achieve its best condition. Herein, a model based on the optimized Monte Carlo method was proposed for effectively analyzing the scattering behavior of electrons within the electron multiplier layer. Unlike traditional simulation, which only deals with the electron scattering in longitudinal, in this paper, we simulate the electron scattering character not only in horizontal but also vertical among the multiplier layer, which would react to the influence induced by structural parameters more complete and more precise. Based on the proposed model, an experimental prototype of EBAPS is built and its detection sensitivity achieves 0.84×10^{-4} lux under spectral response of ultraviolet (UV) spectroscopy, which improved a lot from our former design. The proposed model can be used for analyzing the influence induced by structural parameters, which exhibit enormous potential for exploring the high-gain EBAPS.

Keywords: EBAPS; image sensor; low light level; single photon.

Corresponding author.

1. Introduction

Low-level light single photon imaging (LLLSPI)^{1,2} is used to detect signal as faint as a single photon (the minimum energy of light), and the photonic events amplification (PEA) technology³ is most widely used to achieve LLLSPI. The position and number of every photon would be recorded during the detection by position-sensitive detectors (such as a camera), and the image is formed by continuous accumulation of photons. Due to the high sensitivity of PEA technology, it plays an important role in aerospace.⁴ Besides, it also proves its capability to produce high quality digital output, which shows great potential in scientific research areas such as optical computerized tomography and quantum cryptography.⁵

A lot of methods can be used to achieve PEA. The intensified charge coupled device (ICCD)^{6,7} uses a microchannel plate (MCP) to multiply photoelectrons produced by photocathode. The electron-multiplying charge coupled device (EM-CCD)⁸ uses a gain register to multiply the output signal from the detective device. But these traditional devices suffer from a bulky size, heavy weight, as well as expensive cost.^{9,10} Subsequently, the electron bombarded complementary metal oxide semiconductor image sensor (EB-CMOS-IS)¹¹ was proposed. Compared to the traditional PEA technologies which rely on extra multiplying mechanism, EB sensor is a novel PEA technology which uses impact ionization effect¹² to produce internal multiplying mechanism named Electron bombarded semiconductor (EBS) gain.^{13,14} This can significantly simplify the electron-photon conversion process. Therefore, it is superior in compactness and energy conservation, also with lower noise and enormously improved sensitivity.^{15,16} Nevertheless, limited by the suboptimal device structural parameters and operation parameters, the sensitivity of EB sensor today is far from reaching its maximum potential.¹⁷

In this paper, we optimized the device structural parameters and operation parameters of EBAPS by developing a physical model and analyzing the electron scattering behavior within the electron multiplier layer, and managed to improve its detection sensitivity to a level better than 10^{-4} lux, which improved a lot from our previous design. Besides, unlike the traditional simulation which only deals with the electron scattering in longitudinal, ¹⁸ the model we used is based on the optimized Monte Carlo method, which exhibits a comprehensive simulation of electron scattering behavior not only in horizontal but also in vertical among the multiplier layer. Therefore, the proposed model can be used for further analyzing the influence induced by structural parameters, which exhibit enormous potential for exploring the high-gain EBAPS.

2. Physical Model

The basic structure of EBAPS is shown in Fig. 1. It is an image device made of an EB vacuum system assembled with a backside thinned CMOS (BT-CMOS) image sensor.^{19,20} BT-CMOS is a technology, which reverses the architecture of

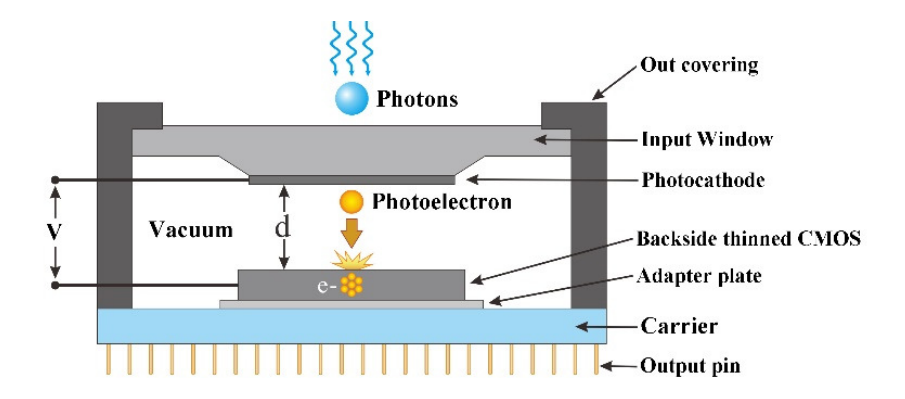


Fig. 1. Schematic diagram of EBAPS.

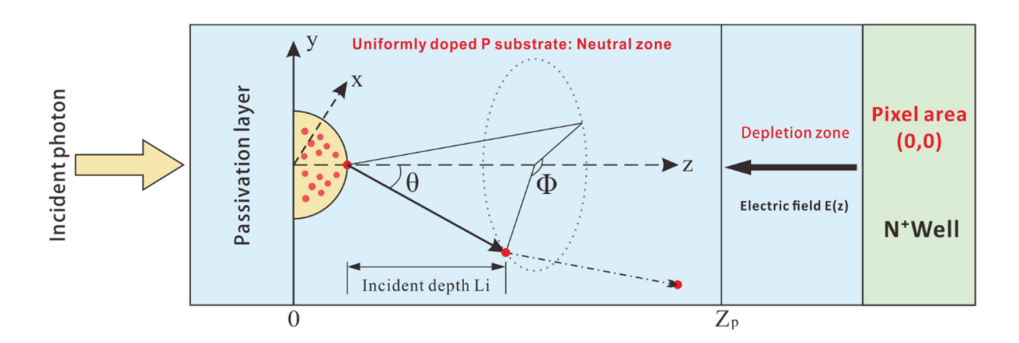


Fig. 2. Multiplication electrons transport model under uniformly doped substrate.

photosensitive layer and substrate layer, enlarging the fill factor to nearly 100%, therefore improving the detection sensitivity, particularly in low-light level conditions. In this system, a photocathode is in proximity focus²¹ with a BT-CMOS. When incident light from input window goes through photocathode, photoelectrons would be produced and then gain enough energy by the applied acceleration voltage between cathode and anode. ¹⁷ Subsequently, high-energy photoelectrons bombard the BT-CMOS, which incur electron multiplication among semiconductor. ²²

In order to study the electron bombarded multiplication principle among the CMOS anode, a physical model is built in what follows.

Figure 2 shows electrons' multiplying, scattering, and collecting process among the multiplication layer.

When photoelectrons bombard CMOSs P-type substrate in high energy, silicon atoms would absorb the energy and trigger the EBS gain.²³ Large numbers of electron-hole pairs are generated and secondary electrons are scattered among the electron multiplication layer. Meanwhile, concentration gradient would make the secondary electrons diffuse from P-type silicon to N well,²⁴ collect and read out by digital current through the output pins.

Electrons' scattering in multiplication layer is mainly formed by elastic scattering and inelastic scattering, ²⁵ elastic scattering only changes the direction of electrons, while inelastic scattering consumes its energy in every collision. When photoelectrons are bombarded into the BT-CMOS, secondary electrons would produce, which would scatter and diffuse among the electron multiplication layer. As the movement of secondary electrons is random, predicting the trajectory for each of them is impracticable. Therefore, the Monte Carlo method²⁶ is used as statistics approaches to analyze this phenomenon.

Assume that the incident photoelectrons satisfy the Gaussian distribution, so the initial coordinate is as follows:

$$\begin{cases} x = \frac{D}{2}\sqrt{-\ln R_1}\cos(2\pi R_2), \\ y = \frac{D}{2}\sqrt{-\ln R_1}\sin(2\pi R_2), \\ z = L \cdot R_3, \end{cases}$$
 (1)

where D is the diameter of incident electron beam, R1 and R2 are random numbers between (0, 1).

For elastic scattering process, we use elastic scattering cross-section formula²⁷ (it suits for low-energy incident electrons of 0.1–30 KeV incident energy).

$$\sigma_T = \frac{3.0 \times 10^{-18} Z^{1.7}}{(E + 0.005 Z^{1.7} E^{0.5} + 0.0007 Z/E^{0.5})} \text{ cm}^2,$$
(2)

where Z is the atomic number, E is the mean electronic energy.

For inelastic scattering, we use energy loss equation proposed by Joy and Lou.²⁸

$$\frac{dE}{ds} = -785 \frac{\rho Z}{AE} \ln \left(\frac{1.166(E + 0.822J)}{J} \right) \text{ eV/Å},$$
 (3)

where ρ is the media density, A is the atomic mass, Z is the atomic number, E is the mean electron energy.

The electrons' scattering among solid states is determined by four factors, i.e. the remaining energy E_n after last time's scattering, scattering angle θ_n , scattering azimuth ϕ_n , and scattering step Λ_n .²⁹ They can be expressed, respectively, as follows:

Electron scattering angle can be expressed as follows:

$$\cos \theta = 1 - \frac{2\beta_i R}{1 + \beta_i - R}, \qquad (4)$$

where R is a random number between (0, 1), β_i is the Rutherford elastic scattering shielding parameter, $\beta i = 3.4 \times 10^3 \frac{Z_i^{2/3}}{E}$, Z is the atomic number and E is the electronic energy.

Scattering azimuth can be expressed as follows:

$$\phi = 2\pi R\,,\tag{5}$$

where R is a random number between (0, 1).

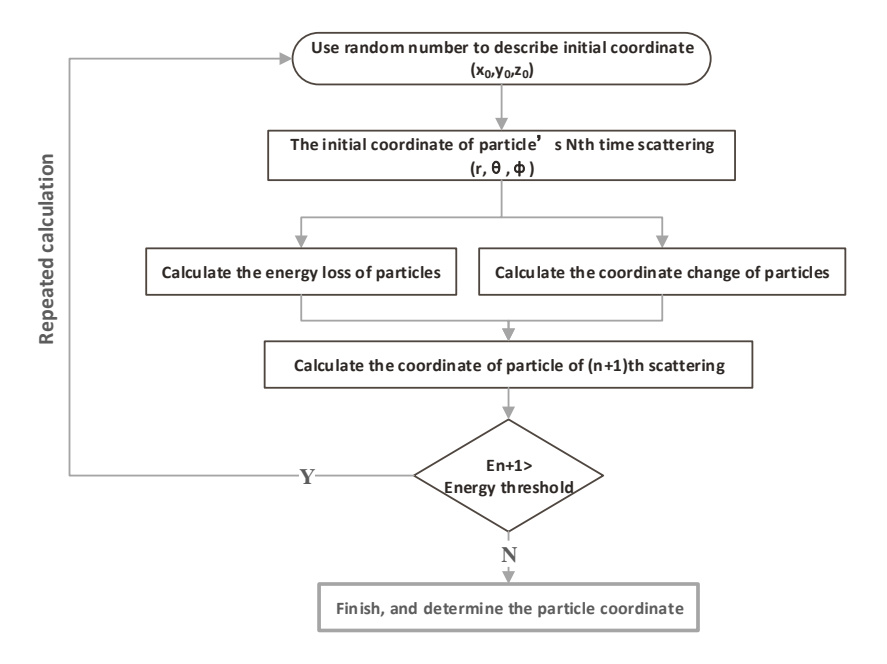


Fig. 3. The Monte Carlo simulation process of incident photoelectrons.

Scattering step can be expressed as follows:

$$\Lambda = -\frac{A}{N_A \rho \sigma_T} \ln R \,, \tag{6}$$

where N_A is the Avogadro constant, that is, 6.02×10^{22} and σ_T is the overall elastic scattering cross-section.

The remaining energy after n times of scattering can be described as follows:

$$E_{n+1} = E_n - \left. \frac{dE}{ds} \right|_{E_n} \cdot \Lambda_n \,. \tag{7}$$

The Monte Carlo method is used to deal with the scattering process, as illustrated in Fig. 3. First, we define the initial coordinate of particle's Nth scattering, then we use the scattering model mentioned above to calculate the energy loss $\frac{dE}{ds}$ and the change of its coordinate. So, the coordinate and remained energy of (n+1)th scattering can be speculated. After that, we compare the electronic energy with the energy threshold (0.1 KeV), only if the remained electronic energy is not greater than the energy threshold. The iteration process would stop and determine the ultimate coordination of electrons. Finally, the electronic trajectory can be calculated.

Based on the above-mentioned model and the simulation process, we can study the influence of the incident photoelectrons' scattering trajectories and secondary electrons' distribution under different parameters such as different incident energy, different incident depth or different diameters of incident electron beam, etc.

3. Simulation Analysis and Results

EBAPS is a device following the proximity focusing principle. Studies demonstrated that the decrease of proximity distance will improve the performance of sensitivity and spatial resolution, while on the other hand, too small proximity distance will also cause high electrical breakdown and introduce extra noise.³⁰ Here, a specific proximity distance of 1 mm is applied to satisfy both high-performance and high-stability.

Under this circumstance, the key point here is to study the influence of incident electrons' energy to the performance of the device.

3.1. The influence of incident electron energy to incident electron bombardment depth

We ignored the B-doping in multiplication layer, and set the thickness of dead layer to 60 nm, the diameter of incident electron beam to 20 nm, and the thickness of P-type epitaxial layer to 10 μ m. The incident photoelectrons' energy is set to 4 KeV and 10 KeV, respectively. The results are as follows.

Electrons' incident depth is a parameter proportionate to the possibility of these electrons detected, the deeper it goes, the more likely it is to be gathered by the N well among the CMOS anode.³¹ Figure 4 indicates that when incident electrons'

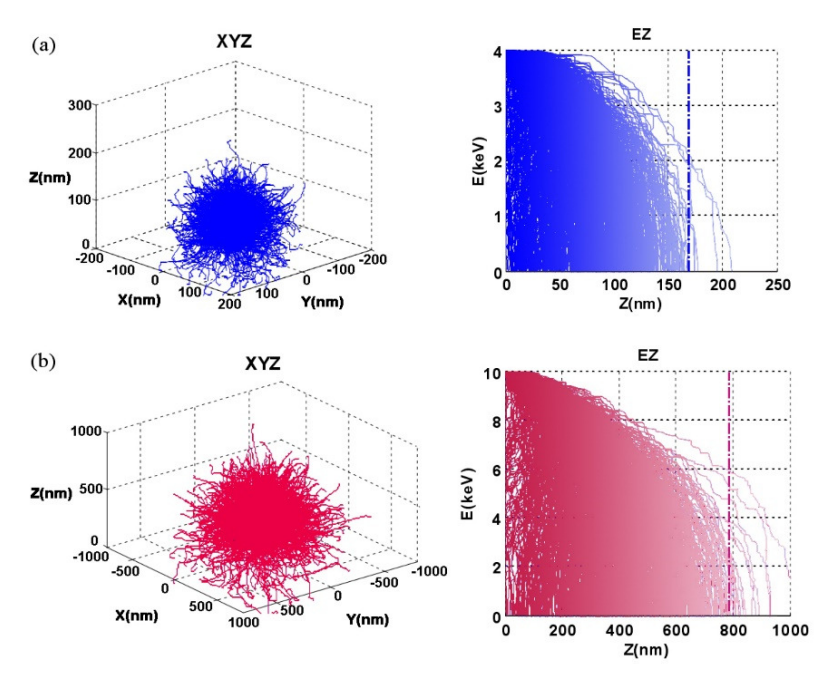


Fig. 4. Electrons' scattering trajectory in multiplication layer (left) and incident electrons' energy consumption in association with incident depth (right) under different incident photoelectron energy. (a) Incident electronic energy of 4 KeV; (b) Incident electronic energy of 10 KeV.

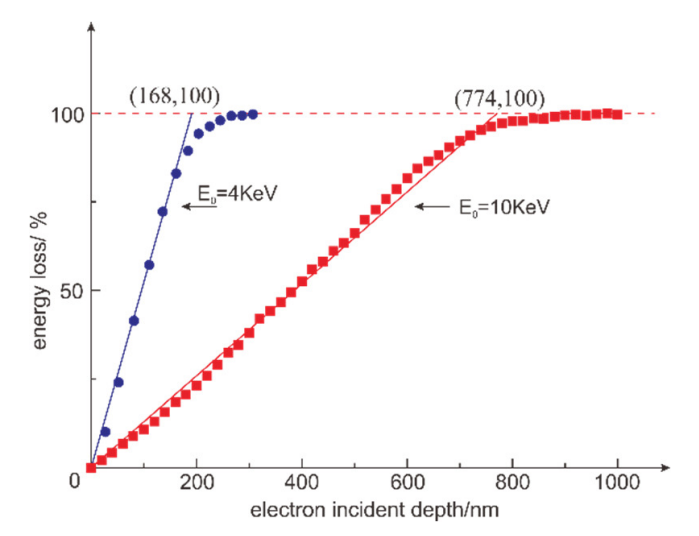


Fig. 5. The simulation result of electron energy loss rate under desperate incident depth.

energy increases from 4 KeV to 10 KeV, the electrons' incident depth increases from 168 nm to 774 nm. In other words, when incident electrons' energy increases by a factor of 2.5, electrons' incident depth increases by a factor of 4.72 (almost doubled the rate of change).

Figure 5 indicates that the incident depth increases with the increase of energy loss rate, which is almost linear. The slope for $E_0 = 4$ KeV is 0.6, the slope for $E_0 = 10$ KeV is 0.13. That is to say, energy attenuation is more rapid when initial energy is relatively low, and the incident depth is way deeper with the increase of initial incident energy.

So, under this circumstance, to make the electronic signal easier to be detected, electrons' initial energy E_0 should be set as high as possible.

However, too high of acceleration voltage would cause breakdown between cathode and anode.¹² Besides, too much of incident electronic energy would also reduce the life span of CMOS detector, or even damage it.³² So, an appropriate accelerating voltage is necessary.

3.2. The influence of incident electron energy to the scattering distribution in XOY plan

Simulation result of scattering distribution in XOY plan is shown in Fig. 6. When incident electrons' energy increases from 4 KeV to 10 KeV, the scattering radius expands from 110 nm to 420 nm. Considering that the diameter of incident electron beam is 20 nm, the scattering magnification is 5.5 and 21, respectively. Meanwhile, as the incident energy increases, the edge distribution gets worse, which would reduce the spatial resolution of low light level imaging.

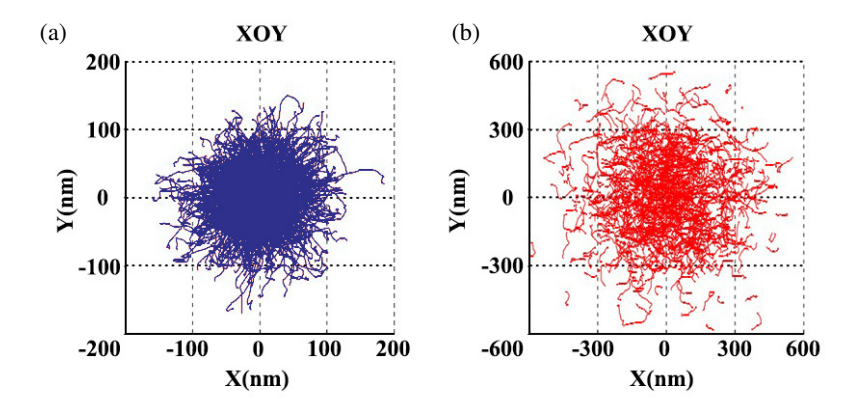


Fig. 6. Electron motion trajectory in XOY plane under different incident photoelectron energy. (a) Incident electronic energy of 4 KeV; (b) Incident electronic energy of 10 KeV.

Table 1. The variation of scattering radius with electron energy.

Incident electrons' energy (KeV)	2	4	6	8	10	12
Scattering radius (nm)	102	110	181	280	450	716
Scattering magnification	5.1	6.0	9.1	13.9	22.5	35.8

The changing trend of scattering radius in XOY plan with the variation of incident electrons' energy is illuminated below. Table 1 shows the variation of scattering radius with the increase of incident electron energy. The scattering magnification indicates that the diffusion magnitude is relative to the incident electron beam (the initial diameter of incident electron beam is 20 nm).

The results demonstrate that when incident electron energy increases, the scattering radius booms dramatically. The corresponding line graph is shown in Fig. 7.

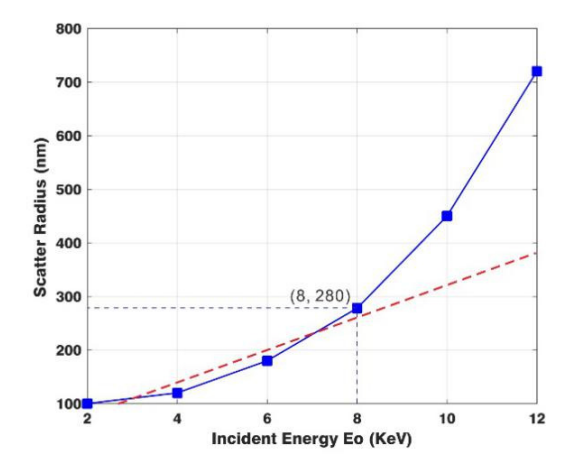


Fig. 7. The scattering radius in XOY plan as a function of incident electron energy.

It indicates that the relation between incident energy and scattering radius is approximately exponential. Unlimited increasing of the incident energy is not advisable because that would cause the scattering radius too big to be localized, and therefore worsen the spatial resolution.

From Fig. 7, we can see that for incident energy under 8 KeV, it has approximately linear incident energy-scattering radius characteristics. So, 8 KeV is chosen as the appropriate incident electron energy. Besides, 8 KeV is also perfectly compatible with both incident depth (630 nm) as well as scattering radius (280 nm). Therefore, 8 kV is what we choose as the ultimate acceleration voltage between photocathode and anode.

3.3. The influence of the thickness of passivation layer to incident electron bombardment depth

Assume that passivation layer is totally made of silica, so for incident electrons, scattering center is either Si or O. The possibility of incident electron interacting with certain atom can be expressed as follows:

$$P_{i} = \frac{C_{i}\sigma_{i}/A_{i}}{\sum_{i=1}^{n} C_{i}\sigma_{i}/A_{i}},$$
(8)

where C_i is the concentration of certain atom, A_i are the atomic weights, σ_i is the scattering cross-section.

Based on this, the incident photoelectrons' energy is set to be 4 KeV, diameter of incident electron beam is set to be 20 nm, and the thickness of P-type epitaxial layer to be 10 μ m. The thickness of passivation layer is set to be 60 nm and 100 nm, respectively. The simulation results are as follows.

Figure 8 indicates that 50 nm of passivation layer still allows most incident electrons to pass through, while 100 nm of passivation layer would almost vanish all the incident energy (4 KeV in this case).

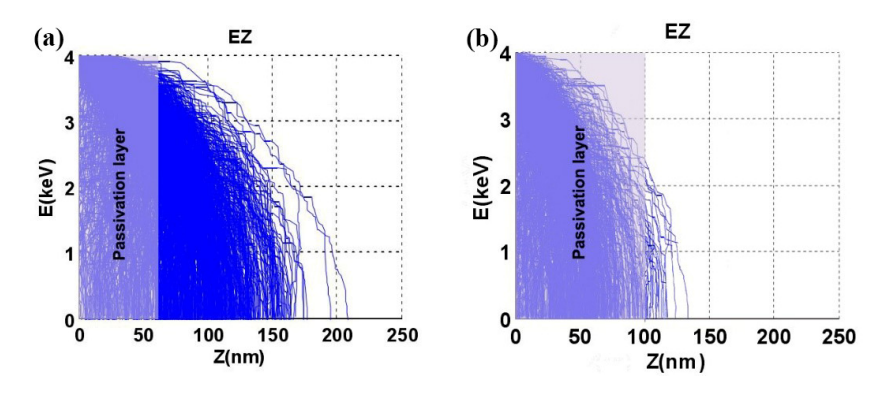


Fig. 8. Electron incident depth under different thickness of passivation layer. (a) passivation layer of 60 nm; (b) passivation layer of 100 nm.

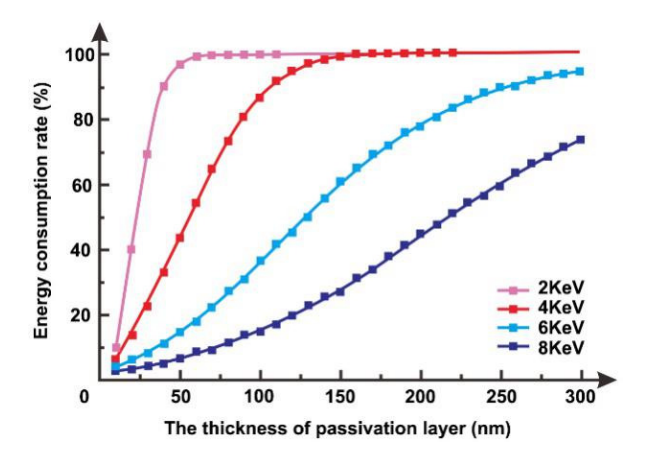


Fig. 9. (Color online) Energy consumption rate changes as the function of the thickness of passivation layer, under different electron incident energy.

More simulations have also been done to achieve the energy consumption rate as the function of the thickness of passivation layer. Figure 9 shows that the energy consumption rate increases proximately linearly with the increase of the thickness of passivation layer. Besides, the increase of electron incident energy would also slow down the energy consumption. In conclusion, the influence of the thickness of passivation layer to electron incident depth is tremendous. So, for EBAPS, the passivation layer should be set as thin as possible in order to increase the charge collection efficiency as well as the electron gain under the same incident electron energy.

Here, thinning technology is used to process the backside illuminated CMOS substrate, as shown in Fig. 10.

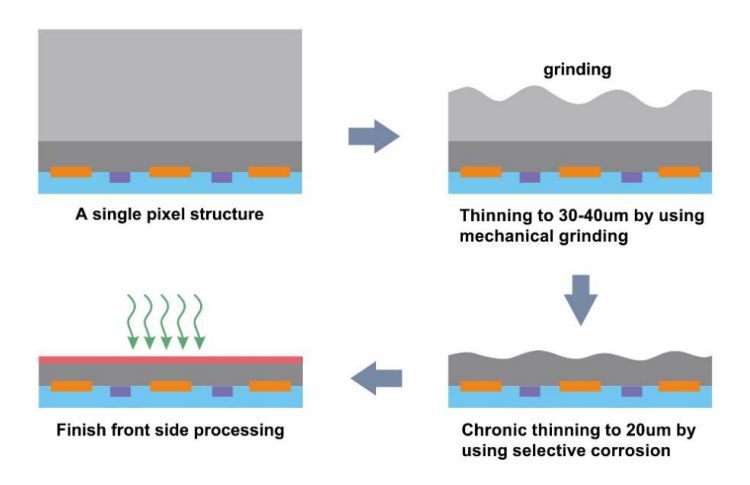


Fig. 10. The thinning technological process of backside illuminated CMOS sensor.

Mechanical grinding is first used to quickly thin the substrate from its original thickness (about 400 μ m) to 30–40 μ m, the chemical corrosion is then used to further thin the substrate to around 20 μ m. Finally, mechanical flattening and polishing is used to process the front side in order to reduce the surface recombination effect and let the produced charge to reach the active region efficiently, therefore maximum enhancing its detection sensitivity.

4. Experimental Verification

Based on the optimized structural parameters and operation parameters of EBAPS, an experimental prototype of EBAPS is built, as shown in Fig. 11. The EBAPS detect component is packaged in a vacuum chamber using a vacuum pump to maintain its vacuum degree under 10^{-9} Pa. Incident light comes from a mercury lamp, which emits ultraviolet (UV) light. In the front side of the incident window, a polarizer filter is assembled to reduce heterogeneous light interference and light intensity, therefore creating a low-light level UV incident light. Inside the vacuum chamber, a gold cathode is used to respond UV incident light and produce photoelectrons, which accelerate by high-voltage power supply. Afterwards, high-energy photoelectrons bombard BT-CMOS and produce large amounts of electron-hole pairs, then read out as output signal.

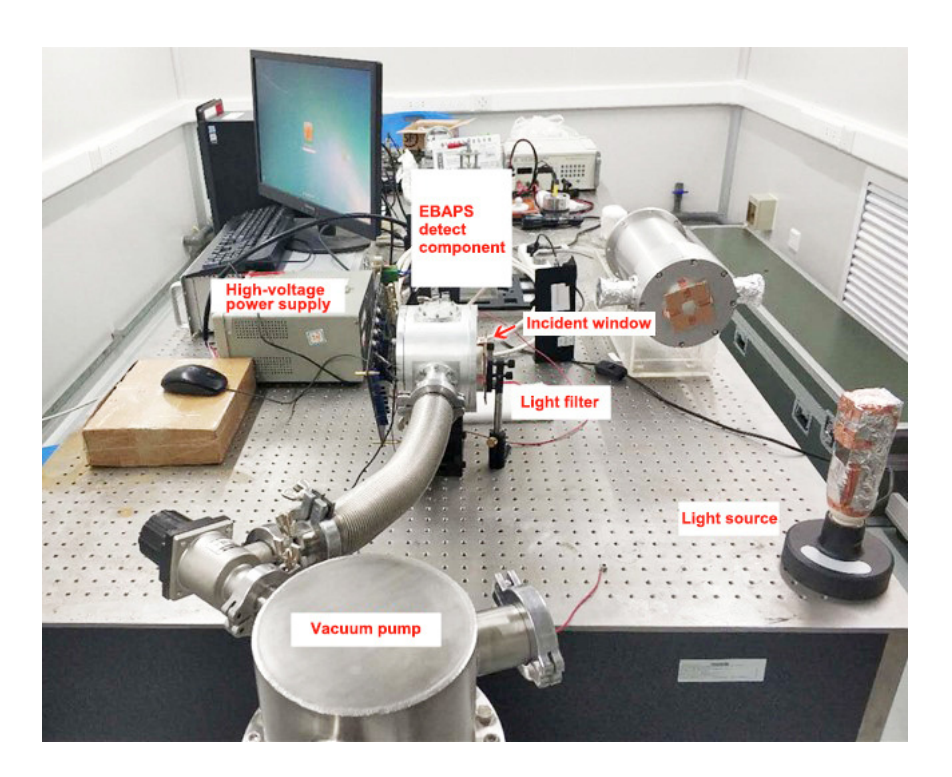


Fig. 11. Schematic diagram of experimental setup.

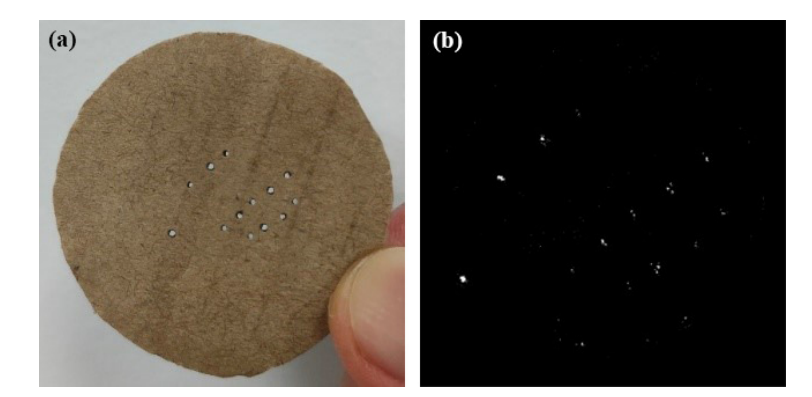


Fig. 12. A frame with low-light level imaging as detected with EBAPS under sensor illuminance of 0.84×10^{-4} lux. (a) A shielding plate placing right before the input window, which has several holes in the middle; (b) The output image of EBAPS after denoising.

In this case, the acceleration voltage between anode and cathode is set to 8 kV, the proximity distance is 1.5 mm, and the thickness of passivation layer is 20 μ m. Based on this, a shielding plate is placed between the incident window and the polarizer filter. The shielding plate has several pinholes on its surface to pass through incident light. The experimental test platform is shown in Fig. 11, and the output image is shown in Fig. 12.

Different intensity of incident light has been tested. When light intensity descends to 0.84×10^{-4} lux, the output signal mark can still be recognized, the output image shows distinguishable light spots, which correspond with the position of pinholes on the shielding plate, indicating that the sensor is operating properly under the given light intensity.

To verify the influence of incident electron energy to the quality of output image, the shielding plate is replaced by a USAF test pattern (Fig. 13(a)). Under the incident light intensity of 0.84×10^{-4} lux, the acceleration voltage of 8 kV is much

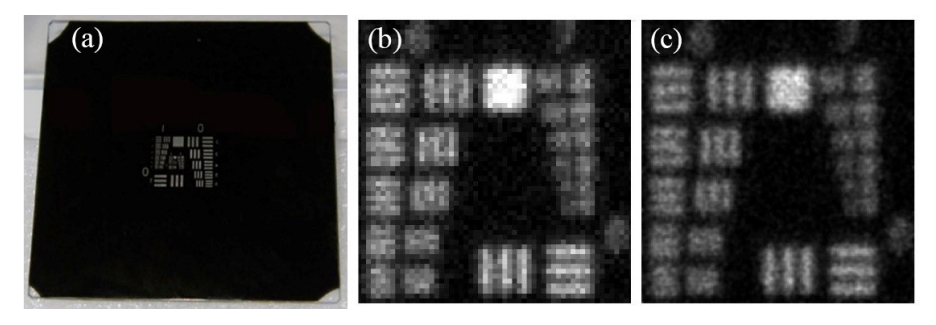


Fig. 13. Images of a USAF test pattern obtained by low-light level imaging with an EBCMOS. (a) the test pattern in use; (b) output image under acceleration voltage of 6 kV; (c) output image under acceleration voltage of 8 kV.

better compared with the acceleration voltage of 6 kV in terms of the quality of output image, as shown in Fig. 13. The result is in accordance with our former simulation, apparently.

5. Conclusion and Perspectives

In conclusion, the optimized Monte Carlo method is studied and applied in the EB-CMOS-IS simulation to analyze the scattering behavior of electrons within the electron multiplier layer. Herein, the scattering characters are simulated horizontally and longitudinally. It is proved to be an important tool to optimize the EB-CMOS-IS manufacturing parameters and its operational conditions. The results show that the incident photoelectron bombardment depth increases linearly with the increase of incident electron energy, and decreases with the thickening of passivation layer. Based on the optimized parameters, an experimental prototype of EBAPS is built and it achieved an improved detection sensitivity of 0.84×10^{-4} lux. Besides, the experimental results correspond to the simulation results very well. It will help further develop the ultrahigh sensitivity EB technology, and exhibit enormous potential for exploring the high-gain EBAPS.

Acknowledgments

This paper was supported by the Shaanxi Natural Science Basic Research Project (No. 2018JM6059), the Equipment Pre-research Field Fund (No. 6140721010203), the West Light Foundation of Chinese Academy of Sciences, (No. XAB2016B25), and thanks to the Key Laboratory of Ultra-fast Photoelectric Diagnostics Technology of CASs help in our research.

References

- W. Verle, EBAPS[®]: Next generation, low power, digital night vision, Int. Symp. OPTRO 2005, 10 May, 2005, France (2005).
- A. Rochas, Single Photon Avalanche Diodes in CMOS Technology, Ph.D. dissertation, EPF-Lausanne, Switzerland (2003).
- 3. G.-Z. Wang, Y. Li and Y.-J. Gao, Chin. J. Electron Devices 21(1) (2008) 308.
- 4. Z. Xiong, Q. Li and Q. Wang, Laser Infrared 42(7) (2012) 725.
- 5. D. J. Denvir, Proc. SPIE 4796 (2003) 164.
- 6. R. Barbier et al., Nucl. Instrum. Methods Phys. Res. A 648 (2011) 266.
- C. D. Mackay, R. N. Tubbs and P. Jerram, Proc. SPIE Int. Soc. Opt. Eng. 4306 (2001) 289.
- 8. A. Rochas et al., Rev. Sci. Instrum. **74**(7) (2003) 3263.
- 9. P. H. Wu, N. Nelson and Y. Tseng, Opt. Express 18(5) (2010) 5199.
- K. B. W. Harpsøe, M. I. Andersen and P. Kjægaard, Astron. Astrophys. 537(2) (2013) 157.
- A. G. Basden, C. A. Haniff, C. D. Mackay et al., A new photon-counting spectrometer for the COAST, SPIE Astronomical Telescopes + Instrumentation (International Society for Optics and Photonics, 2004), p. 677.

J. Bai et al.

- A. Dominjon, M. Ageron, R. Barbier et al., Nucl. Instrum. Methods Phys. Res. A 695 (2012) 172.
- L. Sangalli, N. Partamies, M. Syrjäsuo et al., Int. J. Remote Sens. 32(11) (2011) 2987.
- 14. J. Tian, Infrared Technol. **35**(9) (2013) 527.
- M. Downing, N. Hubin, M. Kasper et al., A declicated L3Vision CCD for adaptive optics applications, in *Scientific Detector for Astronomy 2005*, Vol. 336, eds. J. W. Beletic and P. Amico (Springer, 2006), p. 321.
- T. Brugière, F. Mayer, P. Fereyre et al., Nucl. Instrum. Methods Phys. Res. A 787 (2015) 336.
- R. Barbier, J. Baudot, E. Chabanat et al., Nucl. Instrum. Methods Phys. Res. 610(1) (2009) 54.
- 18. S. Saurabh, S. Maji and M. P. Bruchez, Opt. Express 20(7) (2012) 7338.
- T. Brugière, F. Mayer, P. Fereyre et al., Nucl. Instrum. Methods Phys. Res. 787 (2015) 336.
- 20. O. Jedrkiewicz, J. L. Blanchet, E. Lantz et al., Opt. Commun. 285(3) (2012) 218.
- 21. Y. Yamamoto, Y. Ishikawa, Y. Uraoka et al., Jpn. J. Appl. Phys. 40(12) (2001) 6778.
- 22. J. J. Liou, F. A. Lindholm, J. Appl. Phys. **64**(3) (1988) 1249.
- 23. K. Arisaka, Nucl. Instrum. Methods Phys. Res. A 442 (2000) 80.
- J. Chao, E. S. Ward and R. J. Ober Multidimens. Syst. Signal Process. 23(3) (2012) 349.
- 25. R. Browning, T. Z. Li, B. Chui, J. Ye et al., J. Appl. Phys. 76 (1994) 2016.
- W. J. S. Zhong, J. A. Williams, Etchable core glass compositions and method for manufacturing a high performance microchannel plate: US Patent, US5108961 (1992).
- 27. H. Ren, Y. Mao and S. Li, Ship Electronic Eng. **30**(12) (2010) 87.
- C. Niclass, A. Rochas, P. A. Besse and E. Charbon, IEEE J. Solid-State Circuits 40(9) (2005) 1847.
- 29. G. M. Williams, V. W. Aebi, Proc. SPIE Int. Soc. Opt. Eng. 2415 (1995) 211.
- 30. Y. Wang, P. Yang, W. Zhu et al., Nucl. Electron. Detect. Technol. 21(1) (2001) 31.
- 31. M. S. Robbins and B. J. Hadwen, *IEEE Trans. Electron Devices* **50**(5) (2003) 1227.
- 32. M. Horacek, Rev. Sci. Instrum. 74 (2003) 3379.